Synthesis and properties of [Pt(4-CO2CH3-py)2(dmit)] and [Pt(4-NO2-py)2(mnt)]: Exploring tunable Pt dyes

Cite as:
Moorcraft, L. P., Jack, L. A., Jennings, J. R., Peter, L. M., Yellowlees, L. J., & Robertson, N. (2009). Synthesis and properties of [Pt(4-CO_2CH_3-py)$_2$(dmit)] and [Pt(4-NO_2-py)$_2$(mnt)]: Exploring tunable Pt dyes. *Polyhedron*, 28(18), 4084-4090.

Manuscript received: 06/07/2009; Accepted: 17/09/2009; Article published: 20/09/2009

Synthesis and properties of [Pt(4-CO_2CH_3-py)$_2$(dmit)] and [Pt(4-NO_2-py)$_2$(mnt)]: Exploring tunable Pt dyes**

Lucy P. Moorcraft,[1] Lorna A. Jack,[1] James R. Jennings,[2] Laurence M. Peter,[2] Lesley J. Yellowlees[1] and Neil Robertson[1,*]

[1]EaStCHEM, School of Chemistry, Joseph Black Building, University of Edinburgh, West Mains Road, Edinburgh, EH9 3JJ, UK.

[2]Department of Chemistry, University of Bath, Bath, BA2 7AY, UK.

[*]Corresponding author; e-mail: neil.robertson@ed.ac.uk, tel.: +44 131 6504755, fax: +44 131 6504743

[**]We thank Donald Robertson for providing Na2mnt and Johnson Matthey for supply of K2[PtCl4] for use in this study. Financial support from EPSRC under the Supergen project is gratefully acknowledged. This work has made use of the resources provided by the EaStCHEM Research Computing Facility. (http://www.eastchem.ac.uk/rcf). This facility is partially supported by the eDIKT initiative (http://www.edikt.org).

Supporting information:
Supplementary data associated with this article can be found, in the online version, at http://dx.doi.org/10.1016/j.poly.2009.09.017

Graphical abstract:

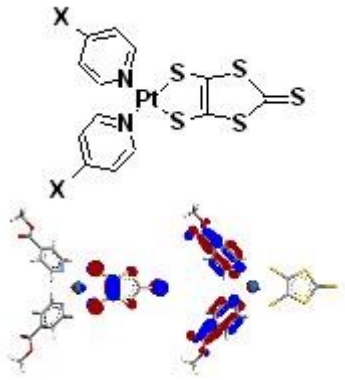

Synopsis:
Square-planar Pt complexes have been prepared and show separate tuning of the HOMO and LUMO orbitals through modification of the dithiolate (HOMO) and pyridyl (LUMO) ligands respectively. This is evidenced by voltammetry, hybrid DFT calculations, UV/Vis spectroelectrochemistry and *in situ* EPR spectroelectrochemistry.

Keywords:
Pt, dithiolate, pyridyl, solar cells, electrochemistry, DFT

Abstract

Two [Pt(II)(substituted-pyridyl)$_2$(dithiolate)] dyes with the formulas [Pt(4-CO_2CH_3-py)$_2$(dmit)] and [Pt(4-NO_2-py)$_2$(mnt)] (where py = pyridyl, dmit = 1,3-dithiol-2-thione-4,5-dithiolate and mnt = maleonitriledithiolate) and their dichloride precursors [$PtCl_2$(4-R-py)$_2$] have been synthesised and compared to a previously reported dye [Pt(4-CO_2CH_3-py)$_2$(mnt)]. Variation of either the pyridyl ligands or the ditholate ligand showed tuning of the electrochemical and spectroscopic characteristics of the dyes as evidenced by cyclic and differential pulse voltammetry, hybrid DFT calculations, UV/Vis spectroelectrochemistry and *in situ* EPR spectroelectrochemistry. The HOMO was shown to be mostly dithiolate based and the LUMO pyridyl based allowing absorption characteristics to be predictably tuned to longer wavelengths, which is important for optimisiation of such dyes in applications such as solar energy conversion.

Introduction

Research on the series of square-planar d^8 [Pt(II)(diimine)(dithiolate)] complexes has shown that systematic modifications to one or both of the ligands can predictably alter the excited state energies by up to 1eV [1]. The high tunability and good photoluminescent properties of these complexes has led to much study of their electronic properties [2], as well as investigation of applications in, for example, photochemical hydrogen production [3] and non-linear optics [4]. An attractive feature of these complexes is the ability to separately tune the energy of the HOMO and LUMO, and hence also the low-energy visible absorption and the excited state energy, by modification of the dithiolate and the diimine respectively. [Pt(II)(diimine)(dithiolate)] complexes are known to show luminescence in fluid solution at ambient temperatures and absorb in the visible region with extinction coefficients ε of 5-10 $kM^{-1}cm^{-1}$. This solvatochromatic LLCT absorption has been described as a "mixed-metal-ligand-to-ligand" charge transfer (MMLL'CT) due to the significant metal character in the dithiolate-based HOMO. Therefore it has been assigned as a (Pt(d)/S(p)/dithiolate → π*/diimine) transition which appears around 450-500nm [1].

The attractive electronic properties of such complexes has also led to their study as dyes for dye-sensitised solar cells [5,6,7,8]. In 1991 O'Regan and Grätzel reported the design of the dye-sensitised solar cell (DSSC) which subsequently showed efficiencies of up to 11% [9,10]. These cells consist of dye molecules, anchored to the surface of nanocrystalline TiO_2, which absorb visible light and inject an electron into the conduction band of the TiO_2 from their excited state. Subsequent reduction of the dye by a redox electrolyte regenerates the dye and the separated electron and hole can be collected at different electrodes. Ruthenium polypyridyl dyes have shown outstanding performance in this type of cell [9].

The synthesis, characterisation and solar cell performance of a family of [Pt(diimine)(dithiolate)] complexes with the general formula [Pt{X,X'-(CO_2R-2,2'-bipyridyl}(mnt)] (where X = 3, 4, or 5, R = H or Et and mnt = maleonitriledithiolate) has been previously reported by us [7]. The 3,3' analogue was found to give a better cell performance due to more favourable recombination energetics than the 4,4' and 5,5' analogues. A steric twist seen in the crystal structure of the 3,3' compound which disrupts the planarity of the bipyridine structure could be a possible cause of this improved performance [8]. This demostrated the pronounced effect on the electronic characteristics of the system through partial decoupling of the two rings of the bpy ligand and prompted our interest in developing this further through analogous complexes with pyridyl ligands. Despite the extensive interest in [Pt(diimine)(dithiolate)] complexes, there has been almost no published research on [Pt$(py)_2$(dithiolate)] (py = substituted pyridyl) complexes but they could offer additional opportunities for fine-tuning the electronic properties due to their greater synthetic flexibility compared to bipyridyl complexes. This could be particularly important in applications such as dye-sensitised solar cells.

We recently studied the complex [Pt(4-CO_2CH_3-py)$_2$(mnt)] **3b** (Scheme 1), the first detailed electronic study of this family of complexes, and demonstrated slow charge recombination of the oxidised dye with electrons injected in TiO_2, similar to that observed with [Pt{3,3'-(CO_2R)-2,2'-bipyridyl}(mnt)] [11]. We noted however that due to the combination of the strongly electron withdrawing mnt^{2-} ligand and the higher energy of pyridyl compared with bipyridyl ligands, the lowest-energy absorption of **3b** was shifted to 390 nm at the edge of the visible region. By substituting the dithiolate ligand or the pyridyl ligands with different analogues, we anticiapte that we can raise the HOMO or lower the LUMO of the dye respectively. This should allow tuning of the low-energy absorption of the absoprtion spectrum of the dye into the visible and properties more appropriate for applications such as solar energy conversion. Here we report such tuning through HOMO and LUMO manipulation involving the synthesis and characterisation of the complexes [Pt(4-CO_2CH_3-py)$_2$(dmit)] and [Pt(4-NO_2-py)$_2$(mnt)] (dmit = 1,3-dithiol-2-thione-4,5-dithiolate) and compare these to **3b** that we previously reported as well as the respective dichloride precursors [$PtCl_2(py)_2$]. We also report preliminary investigation of the sensitisation of TiO_2 with these dyes.

Results and Discussion

Synthesis

The [Pt$(py)_2$(dithiolate)] complexes [Pt(4-X-py)$_2$(mnt)] and [Pt(4-X-py)$_2$(dmit)] (X = CO_2CH_3 and NO_2) were synthesised using the routes shown in Scheme 1. Complexes **2c**, **3c**, **4a** and **4b** are new to this work and will be compared with **2a**,**b** and **3a**,**b** that we have reported previously [7]. Reaction of two molar equivalents of the 4-CO_2R-py or 4-NO_2-py ligand precursors (**1a-c**) with potassium tetrachloroplatinate

gave the dichloro-substituted platinum complexes and further reaction of these with the disodium salt of mnt^{2-} or $dmit^{2-}$ gave the target products. We were unable to prepare **4c** in good purity, possibly due to easy formation of $[Pt(dmit)_2]^{x-}$ side product that contaminated samples and altered desired reaction ratios. For synthesis and isolation of **4a** and **4b**, this factor was overcome with careful optimisation of the best reaction conditions.

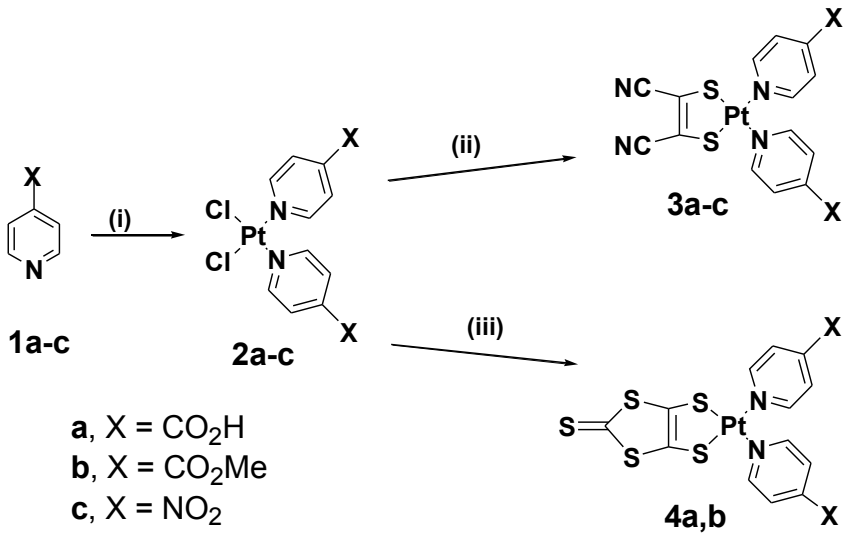

Scheme 1. Synthesis of $[Pt(4\text{-X-py})_2(\text{dithiolate})]$ complexes where dithiolate = mnt^{2-} and X = CO_2H (**3a**), CO_2Me (**3b**), NO_2 (**3c**); dithiolate = $dmit^{2-}$ and X = CO_2H (**4a**) and CO_2Me (**4b**) from the precursor complex $[PtCl_2(4\text{-X-py})_2]$ (**2a-c**) and uncomplexed pyridyls (**1a-c**). (i) $K_2PtCl_{4(aq)}$, reflux (ii) Na_2mnt, RT.(iii) Na_2dmit, RT.

The ester complex **4b** was synthesised to aid the characterisation of the dye molecules as they show greater solubility in a wider range of solvents. The acid analogue **4a** and the mnt^{2-} complex **3a** previously published were synthesised as this form can be readily bound to TiO_2 for testing in a solar cell or other photoelectrochemical applications. We also explored the utility of the NO_2-substituted complex **3c** for sensitisation of TiO_2 and as a solar-cell dye as the nitro group has not to the best of our knowledge previously been investigated in binding dyes to oxide semiconductors.

Electrochemistry

The electrochemistry of **2c**, **3c** and **4b** were studied using cyclic voltammetry and compared with the previously-reported **2b**, **3b** and the ligand precursor **1c** (Table 1). Complex **4b** (in a solution of 0.1 M

$TBABF_4$ / DMF) shows two pyridyl-based reversible reduction peaks at -1.13 V amd -1.31 V and an irreversible oxidation at 1.11 V (Figure S1). The consistency of these reduction potentials with those of **3b** and **2b** [11] shows that reduction of this complex is based on the pyridyl ligands. The absence of an oxidation process for **2b** in comparison with **4b** suggests the HOMO of the latter is located on the $dmit^{2-}$ ligand as expected. The lower oxidation potential for **4b**, in comparison with **3b**, arises from the less electron withdrawing character of the $dmit^{2-}$ ligand compared with mnt^{2-} and this leads to a smaller separation between the first reduction and oxidation potential for **4b** compared with **3b**.

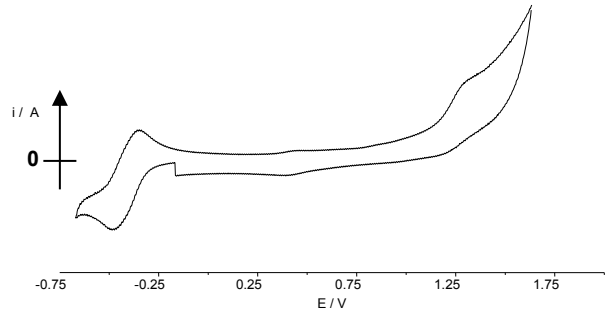

Figure 1. Cyclic voltammetry of [Pt(4-NO_2-py)$_2$(mnt)] **3c** in 0.1 M $TBABF_4$ / DMF at 298 K. Scan Rate = 0.1 V s^{-1}.

Table 1. Oxidation and Reduction potentials for **4b**, **3c** and **2c** vs Ag/AgCl in solutions of 0.1 M $TBABF_4$ / DMF at 298 K. Data for **3b**, **2b** and **1c** are shown for comparison. The reductions were chemically and electrochemically reversible (as evidenced by straight line plots of i_{max} vs (scan rate)$^{1/2}$) and values indicate $E_{1/2}$. Oxidations were chemically irreversible and values indicate peak potential.

Compound	$E^{red}(2)$/V	$E^{red}(1)$/V	E^{ox}/V	E^{ox}-$E^{red}(1)$/V
4b	-1.31	-1.13	1.11	2.24
3b[11]	-1.25	-1.10	1.24	2.34
2b[11]	-1.32	-1.15	-	-
3c	-0.47	-0.44	1.28	1.72
2c	-0.47	-0.44	-	-
1c	-	-0.74	-	-

[Pt(4-NO_2-py)$_2$(mnt)] **3c** and the dichloride precursor complex [$PtCl_2$(4-NO_2-py)$_2$] **2c** were studied using cyclic (Figure 1) and differential pulse voltammetry. An electrochemically reversible reduction peak at -0.46 V, observed by cyclic voltammetry for both complexes, is consistent with a two-electron reduction based on the two attached nitropyridine ligands. Differential pulse voltammtery (Figure S2) shows that the broad peak seen in the cyclic voltammetry actually consists of two closely-spaced reductions at -0.44 V and -0.47 V respectively. Cyclic voltammetry of **3c** also shows an oxidation at 1.28 V assigned by

analogy as based on the mnt^{2-} ligand. For **2c** and **3c**, a typical shift to less negative potential is seen in comparison with **1c** (Figure S3) due to interaction with the electron-withdrawing Pt centre. This is similar to the series **1b** – **3b**, although less pronounced for the nitro series. This is explained by the large NO_2-character of the LUMO for **2c** and **3c** (*vide infra*) which lessens the effect of complexing to Pt.

DFT Calculations and Spectroelectrochemistry.

Hybrid DFT calculations (see Experimental section) for [Pt(4-CO_2CH_3-py)$_2$(dmit)] **4b** (Figure 2) show that the HOMO is based on the dmit ligand and has 5.20 % Pt character. The LUMO is determined to be distributed over both the pyridyl-ligands and also has 3.12 % Pt character. The next highest orbital is found, within the limits of the calculation, to have the same energy as the LUMO and is also distributed over both pyridyl ligand indicating that the molecule effectively has two degenerate LUMO orbitals. A summary of Pt, py and dithiolate contributions to the frontier orbitals is given in Table 2 and full details of energies and atom contributions can be found in the Table S1. It should be noted that in our previous computational study of **3b** [11], the location of the LUMO orbital was found to vary with the angle between the pyridyl ligands; if this were contrained to 90 degrees then the two degenerate LUMOs were on separate py ligands but if the angle were less then the degenerate LUMOs were each spread over both py ligands. The former was found to be unambiguously consistent with the experimental EPR data. In the current computational study for both **4b** and **3c**, we found that the degenerate LUMOs were always spread over both py ligands, even if the angle were constrained to 90 degrees. From the EPR study however (*vide infra*), this seems to be an artefact of the calculation as the EPR clearly demonstrates one degenerate LUMO located on each pyridyl ring as in the prior study of **3b**.

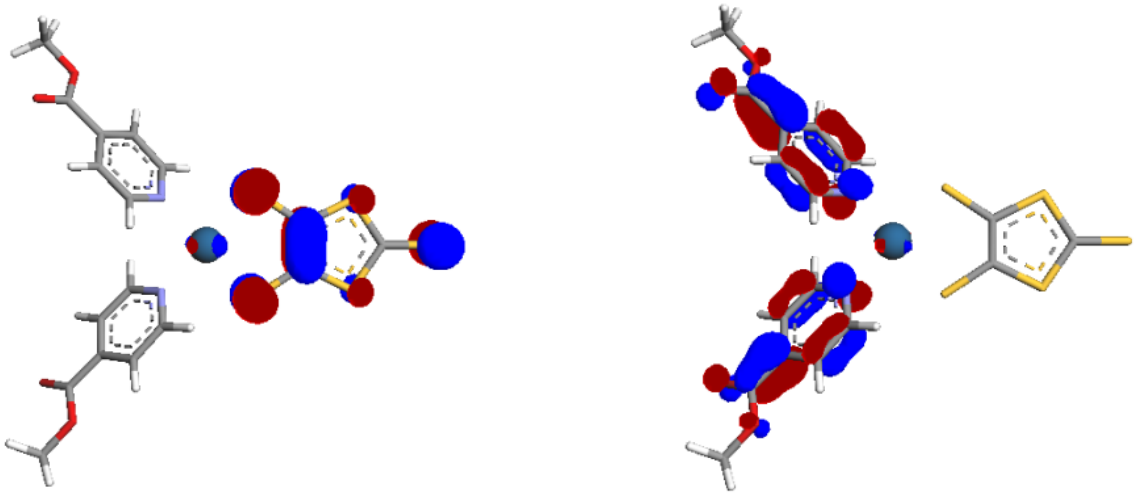

Figure 2. The HOMO (left) and the LUMO (right) isosurfaces for [Pt(4-CO_2CH_3-py)$_2$(dmit)] **4b** from hybrid DFT calculations

Table 2. Percentage contribution for the platinum, pyridine and ditholate components in the HOMO and LUMO of **4b**, **3c** and **3b** [11] determined from hybrid DFT Calculations.

Compound	Orbital	Contribution		
		Pt	pyridines	ditholate
Pt(4-CO_2CH_3-py)$_2$(dmit)] **4b**	HOMO	5.35	5.45	89.20
	LUMO	3.12	94.13	2.75
Pt(4-NO_2-py)$_2$(mnt)] **3c**	HOMO	11.87	7.68	80.45
	LUMO	2.51	94.80	2.69
Pt(4-CO_2CH_3-py)$_2$(mnt)] [11] **3b**	HOMO	12.60	6.04	81.36
	LUMO	2.81	95.22	1.97

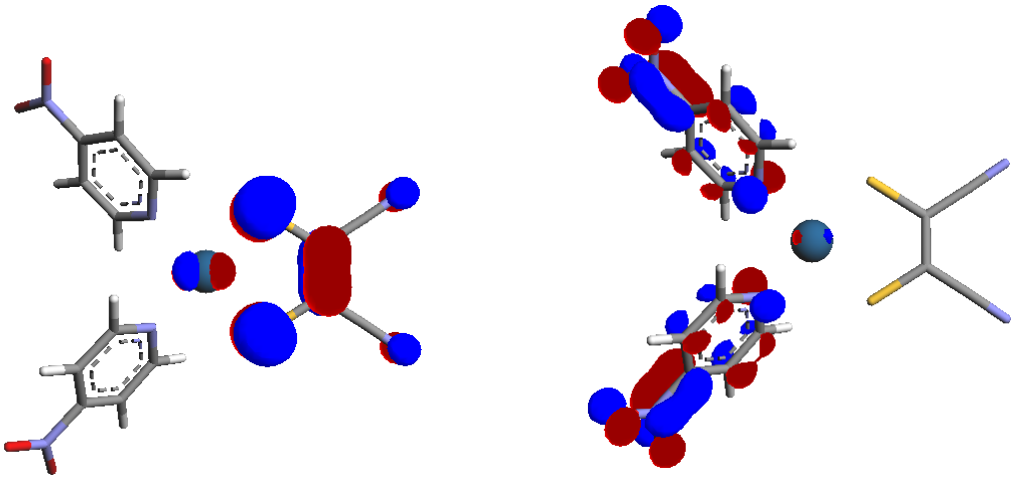

Figure 3. The HOMO (left) and the LUMO (right) isosurfaces for [Pt(4-NO_2-py)$_2$(mnt)] **3c** from hybrid DFT calculations.

Hybrid DFT calculations for [Pt(4-NO_2-py)$_2$(mnt)] **3c** (Figure 3, Table 2) again show the HOMO is based on the dithiolate (mnt^{2-}) ligand although with 11.54 % Pt contribution, similar to **3b** which also contains the mnt^{2-} ligand. It is noticable that both **3b** and **3c** show considerably more Pt contribution to the HOMO than the $dmit^{2-}$ complex **4b**. The LUMO and LUMO+1 of **3c** are degenerate within the limits of the calculation and are based over both pyridyl-ligands as was seen for **4b,** with Pt contribution of 2.49% for the LUMO and, in noticable contrast to **3b**, much of the orbital (44%) situated on the NO_2 groups of the ligands. This highlights the strong electron-withdrawing character imparted to the pyridyl ligands through substitution with the nitro group and is consistent with the less negative reduction potentials in comparison with the carboxyester-substituted **2b** and **3b**, and the smaller shift in reduction potential of **2c**, **3c** compared with **1c**. Full details of energies and atom contributions can be found in Table S2.

TD-DFT calculations were carried out for [Pt(4-CO_2CH_3-py)$_2$(dmit)] **4b** and [Pt(4-NO_2-py)$_2$(mnt)] **3c** in the presence of DMF and used to aid interpretation of the UV/Vis spectra. This method has been

previously used on similar platinum-diimine-dithiolate systems with the results showing a good similarity to experimental observations [8,11]. It should be noted that the inclusion of solvent in these calculations is essential, as has been observed previously in similar systems [12], as the TD-DFT studies carried out in vacuum vastly underestimated the energy of the lowest energy transition. A summary of relevant calculated transitions for each complex can be found in Tables S3 and S4 and the calculated transitions relative to the observed absorption spectrum are shown in Figures 4 and 5. The positions and relative size of the oscillator strengths in the TD-DFT calculations match the observed spectra reasonably well. Firstly, we can note that both complexes show a significant low energy visible absorption at 20600 cm^{-1} (485 nm, **4b**) and 22000 cm^{-1} (454 nm, **3c**). This demonstrates the success of the strategy to tune the absorbance at 25700 cm^{-1} (390 nm) for **3b** into the visible spectrum through manipulation of the HOMO (**4b**) and LUMO (**3c**) respectively. Interestingly, the calculated composition of the lowest energy intense transition was found to be mostly HOMO – LUMO+2 (predominantly pyridyl-ring based) for both **3c** and **4b** and this is in keeping with calculations for **3b** [11], allowing assignment of the low-energy transition as LLCT. Thus is each case, the transition from the HOMO to the degenerate pair of LUMO orbitals is found to be very weak, for example in **3c** it is calculated to have oscillator strength only 10% that of the HOMO – LUMO+2 transition. Due to this, the colour tuning of **3c** is less effective than that of **4b** since the effect of the nitro substituents has a larger effect on the degenerate LUMO orbitals rather than the LUMO+2, with coefficients on the nitro groups for the latter close to zero. The HOMO – LUMO transition for **3c** is indeed calculated to be tuned to long wavelength (15200 cm^{-1}, 656 nm, Fig. 5) but due to its low intensity has negligible effect on the spectrum. The visible absorption observed for **3c** seems due only to some broadening of the HOMO – LUMO+2 transition. All the other intense transitions calculated for **3c** are charge-transfer in character, from orbitals mostly based on the PtS_2 fragment to orbitals based on the py ligands.

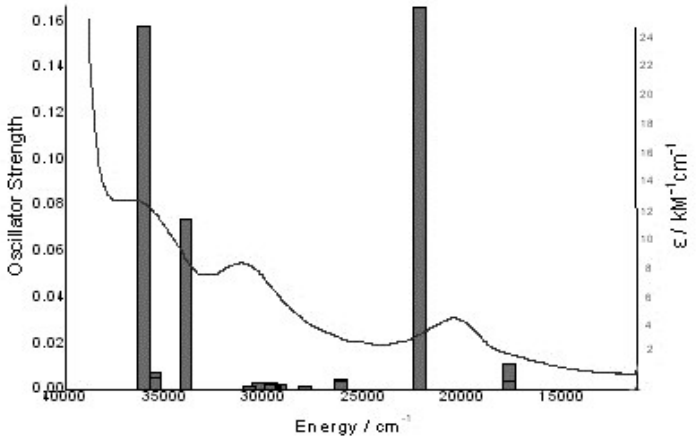

Figure 4. Calculated transitions and observed spectrum for [Pt (4-CO_2CH_3-py)$_2$(dmit)] **4b.**

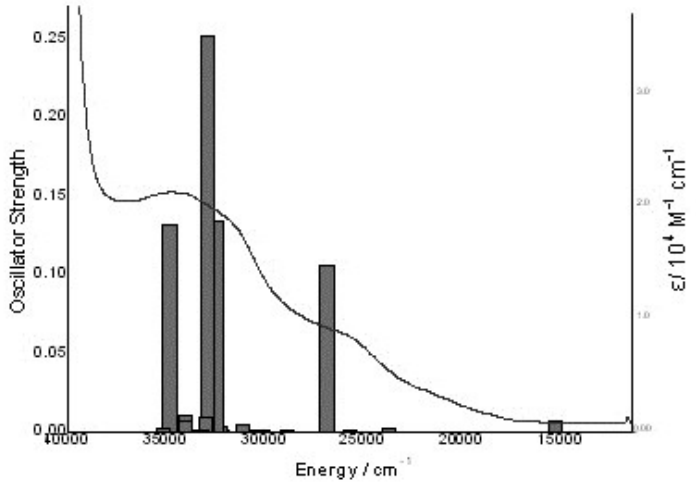

Figure 5. Calculated transitions and observed spectrum for [Pt(4-NO_2-py)$_2$(mnt)] **3c.**

Table 3. UV-Vis bands for the neutral compounds Pt(4-CO_2CH_3-py)$_2$(dmit)] **4b**, Pt(4-NO_2-py)$_2$(mnt)] **3c** and Pt(4-CO_2CH_3-py)$_2$(mnt)] [11] **3b**. Experimental spectra were taken in solutions of 0.1 M $TBABF_4$ / DMF at 233 K.

Compound	Peak Position / cm^{-1}(ε / $M^{-1}cm^{-1}$)		
Pt(4-CO_2CH_3-py)$_2$(dmit)] **4b**	36,100 (12,300)	31,100 (8,100)	20,600 (4,300)
Pt(4-NO_2-py)$_2$(mnt)] **3c**	33,600 (20,000)	30,700 (17,000)	25,000 (7,500) 22,000 (shoulder)
Pt(4-CO_2CH_3-py)$_2$(mnt)] **3b**	36,300 (13,500)	31,600 (10,000)	25,700 (5,400)

UV/Vis/NIR spectroelectrochemistry of **4b** and **3c** (Fig. 6, Fig. 7) was performed to gain further information on the frontier orbitals of the complexes. This involved electrochemical reduction to mono- and di-reduced and oxidation to mono-oxidised states. Comparison with related studies for **1c**, **2c** (Figure S4, S5) and **3b** gave some insight into transition processes. Upon reduction of **4b** to the mono- and di-reduced species (Figure 6), the peak at 36100 cm^{-1} is retained; the peak at 31100 cm^{-1} increases in intensity and shifts slightly to lower energy and a new band at 24000 cm^{-1} grows in. In keeping with results for **3b** [11], the lowest energy peak is still observed and does not collapse upon population of the degenerate LUMO orbitals upon reduction. This is consistent with our assignment of this as HOMO – LUMO+2 from the computational study. Also in keeping with **3b**, the second reduction involves no change in the number of peaks compared with the first but just involves growth of the existing peaks. This is also interpreted as the sequential addition of electrons to each degenerate LUMO orbital. The

similarities between **4b** and **3b** reflect the common character of the 4-CO_2Me-py based LUMO orbitals in each.

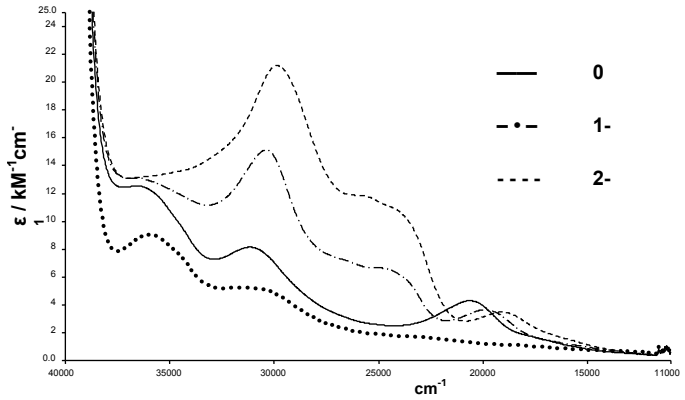

Figure 6. Spectroelectrochemistry of [Pt(4-CO_2CH_3-py)$_2$(dmit)] **4b** in 0.1 M $TBABF_4$/ DMF at 233 K. E_{gen} = -1.2 V(1-), -1.6 V(2-) and 1.5 V (1+).

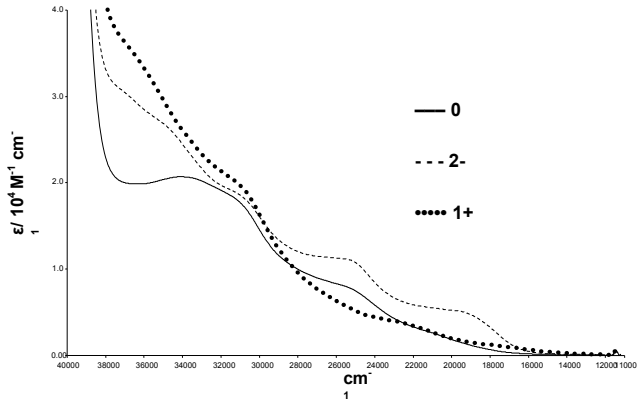

Figure 7. Spectroelectrochemistry of [Pt(4-NO_2-py)$_2$(mnt)] **3c** in 0.1 M $TBABF_4$ / DMF at 233K. E_{gen} = 1.0 V (2-) and 1.5 V (1+).

For [Pt(4-NO_2-py)$_2$(mnt)] **3c** (Figure 7), upon reduction to the di-reduced species, the bands at 30700 cm^{-1} and 25000 cm^{-1} increase in intensity and peaks at 35000 cm^{-1} and 19000 cm^{-1} grow in. This is similar to the [$PtCl_2$(4-NO_2-py)$_2$] **2c** precursor which had peaks grow in at 30300 cm^{-1}, 25800 cm^{-1} and 19200 cm^{-1}. It is readily apparent that there is a qualitative difference between reduction of **3c** and **4b**/**3b** due to the location of the LUMO orbitals on the 4-NO_2-py ligands in the former. Also, as the sequential pyridine

reductions in **3c** occur at very similar potentials it was not possible to generate the mono-reduced species. Upon oxidation of **3c**, a peak at 36000 cm^{-1} grows in, the 30700 cm^{-1} band increases intensity and 25000cm^{-1} loses intensity. A weak low energy band at 16500 cm^{-1} also appears.

In situ EPR

In situ EPR studies of **4b** and **3c** were carried out and compared with related complexes. This involved reduction of the complexes to the dianionic states and the simultaneous measurement of the EPR spectrum. The simulation parameters for the spectra along with [11] $\mathbf{3b}^{2-}$ and the dichloride precursor compounds $\mathbf{2b}^{2-}$ and $\mathbf{2c}^{2-}$ are reported in Table 4. The direduced complex $[Pt(4\text{-}CO_2CH_3\text{-}py)_2(dmit)]^{2-}$ $\mathbf{4b}^{2-}$ remains EPR active, showing that the electrons enter two separate orbitals (the LUMO and LUMO+1) based on the pyridyl ligands, as they do in the dichloride precursor complex and the mnt analogue. This contrasts with analogous bipyridyl complexes [Pt(substituted-bipy)(dithiolate)] where both reduction electrons enter the same orbital and the dianion is EPR silent [8]. The spectrum obtained was not sufficiently resolved to determine any couplings other than to Pt at 54 G and to one aromatic nitrogen at 6.8 G. This is very similar to the couplings found for $\mathbf{2b}^{2-}$ and $\mathbf{3b}^{2-}$ (Table 4). Importantly, the coupling to only one nitrogen nucleus indicates unambiguously that the SOMO is based on only one pyridyl ligand rather than being delocalised over both in contrast to the calculation. As noted above however, this aspect of the calculations has previously been shown to be very susceptible to slight differences in starting geometry and is not reliably determined [11].

Table 4. EPR Simulation Parameters for $[Pt(4\text{-}CO_2CH_3\text{-}py)_2(dmit)]^{2-}$ $\mathbf{4b}^{2-}$, $[PtCl_2(4\text{-}NO_2\text{-}py)_2]^{2-}$ $\mathbf{2c}^{2-}$ and $[Pt(4\text{-}NO_2\text{-}py)_2(mnt)]^{2-}$ $\mathbf{3c}^{2-}$ (Figure S6-8), and for comparison $[PtCl_2(4\text{-}CO_2CH_3\text{-}py)_2]^{2-}$ $\mathbf{2b}^{2-}$ and $[Pt(4\text{-}CO_2CH_3\text{-}py)_2(mnt)]^{2-}$ $\mathbf{3b}^{2-}$ in 0.1 M $TBABF_4$ in DMF at 233 K. All hyperfine coupling constants are given in G. Δ = linewidth. *Carried out in 0.3 M $TBABF_4$ / DCM.

	$\mathbf{2b}^{2-}$	$\mathbf{3b}^{2-}$	$\mathbf{4b}^{2-}$	$\mathbf{2c}^{2-}$*	$\mathbf{3c}^{2-}$
a_{iso}(Pt)	55.5	41.0	54.0	34.0	29.0
a_{iso}(N)	6.7	6.725	6.8	5.4	7.9
a_{iso}(N)	-	-	-	4.1	5.1
2 x a_{iso}(H)	-	-	-	2.68	2.784
g	2.0003	2.0043	1.9992	2.0055	2.0068
Δ	5.75	5.5	10.0	0.7	1.1

For $[Pt(4\text{-}NO_2\text{-}py)_2(mnt)]^{2-}$ $\mathbf{3c}^{2-}$, the dianion is again EPR active indicating that the electrons again enter the degenerate LUMO and LUMO+1 orbitals. Coupling is observed with the Pt(II) centre and to two

nitrogen atoms on the pyridine ligands. The coupling to the platinum (II) centre has decreased to 29 G compared with 34 G for the dichloride precursor complex **2c** and the electron-withdrawing character of the nitro-pyridines appears to reduce the Pt character in the LUMO compared with **2-4b**. Overall from the EPR results, the percentage Pt contribution to the SOMO increases in the order $\mathbf{3c}^{2-} < \mathbf{2c}^{2-} < \mathbf{3b}^{2-} < \mathbf{4b}^{2-} < \mathbf{2b}^{2-}$. This trend is in keeping with the calculated Pt contribution to the respective LUMOs which increases in the order **3c** < **3b** < **4b**.

The couplings to the nitrogen atoms on the substituted pyridine ligands have increased from 5.4 G and 4.1 G ($\mathbf{2c}^{2-}$) to 7.9 G and 5.1 G ($\mathbf{3c}^{2-}$). *In situ* EPR ^{15}N-labelling experiments [13] on 4-$^{15}NO_2$-py have confirmed that in this compound, it is the nitrogen in the NO_2 group that the electron couples more strongly to, although it is not possible to determine definitely which coupling corresponds to which nitrogen in the [Pt(4-NO_2-py)$_2$(mnt)] complex. Note however, that the observations of two dissimilar N-couplings indicates that the SOMO is based on only one of the pyridyl ligands analogous to $\mathbf{4b}^{2-}$ and $\mathbf{3b}^{2-}$, since coupling to either four nitrogen nuclei or two equivalent nitrogen nuclei would be observed if the SOMO were delocalised over both pyridyls. Furthermore we can conclude from the similarity of the two couplings to nitrogen nuclei that the reduction electron enters an orbital that is significantly based on the nitro group.

Oxide Sensitisation Studies

The shift to positive potential for the first reduction of **3c** in comparison with **3b** suggests that the former is not likely to be able to inject electrons into the conduction band of TiO_2 in a solar cell. Nevertheless we explored the possibility to prepare DSSC using **3c** (Table S5) in case some alteration to the energy levels occurred upon binding to TiO_2. We were also interested to explore in general whether nitro groups could in principle provide stable attachment to an oxide semiconductor analogous to carboxy groups as this might open up other possible applications in oxide modification, e.g. in photocathodic processes. Through soaking a slide of nanocrystalline TiO_2 with **3c** in a variety of solvents, in particular methanol, we were able to bind the dye to the semiconductor leading to a coloured film (Figure 8). Solar cell performance was extremely poor however and, in addition to concerns over the inappropriate LUMO energy, the dye was found to desorb substantially from the semiconductor when in contact with the redox electrolyte solution used to fabricate the solar cells (Figure 9). Interestingly, this process was dependent not only on the presence of solvent, but on the specific electrolyte species dissolved. TBP and LI both lead so some desorption of the dye in comparison with methanol solution, however I^-/I_3^- appeared in particular to lead to significant desorption of the dye. These results clearly indicate that, in the presence of liquid electrolyte, the nitro group is poorer at binding the dye to TiO_2 in comparison with the established carboxy group. This suggests that futher work using nitro groups as anchors for oxide

semiconductors might best combine these with carboxy or other acid groups to enable energy level tuning combined with sufficient binding strength for practical use.

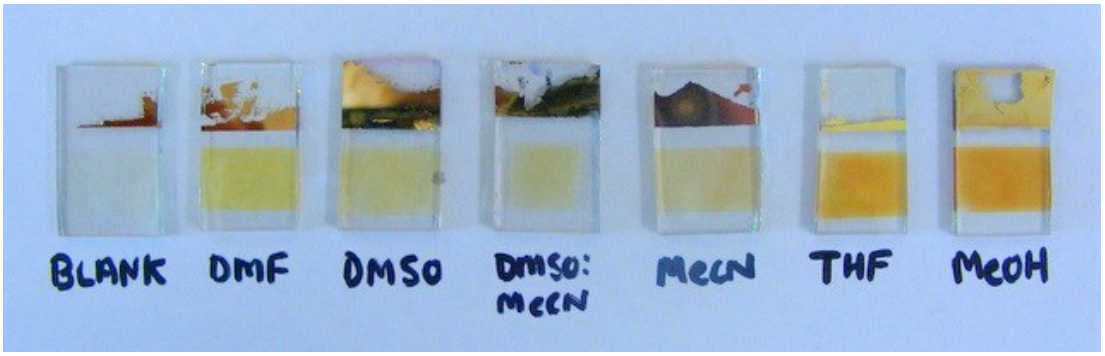

Figure 8. Sensitisation of TiO_2 slides by **3c** left in various solvent dye baths for 48 h (unsensitised, DMF, DMSO, DMSO:CH_3CN (1:1), CH_3CN, THF and methanol respectively) . The nanocrystalline TiO_2 area is the rectangle in the lower portion the slide.

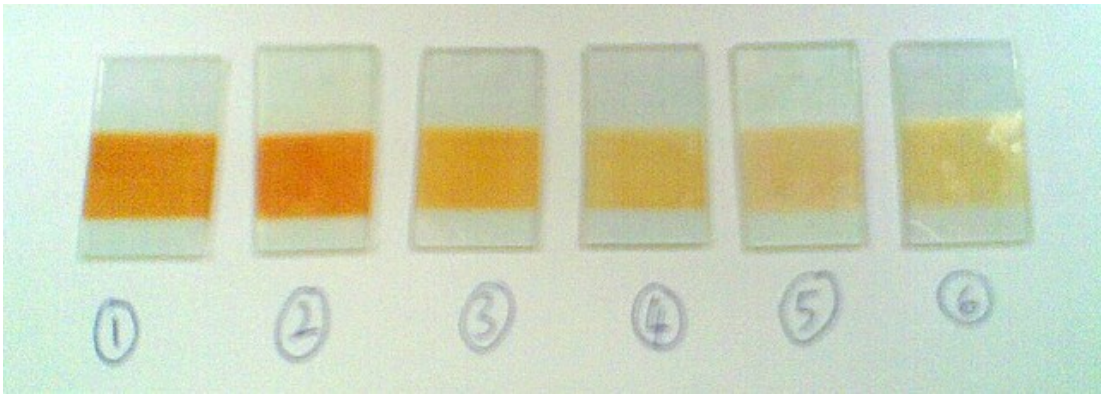

Figure 9. Slides of TiO_2 senstised with **3c** after exposure to various electrolyte components: (1) MeOH (2) 3-MPN (3) 3-MPN + TBP (4) 3-MPN + LiI (5) 3-MPN + LiI + I_2 (6) 3-MPN + LiI + I_2 + TBP. (3-MPN = 3-methoxy propionitrile, TBP = 4-tert-butylpyridine).

More surprisingly, dye **4a** was also found to display a poor performance in a DSSC (Table S5) despite the presence of the typical carboxy anchoring group, visible charge transfer absorption and redox potentials suitable for DSSC function. Although not as apparent as for **3c**, some loss of dye was observed upon exposure of the sensitised film to solutions of TBP (Figure S9) suggesting that there may be some inherently lower stability in the pyridyl dyes anchored to TiO_2 in comparison with bipyridyl dyes. This could reflect the monodentate character of the pyridyl complexes which could lead to lower stability in

comparison with bidentate bipyridyl ligands. In future studies this may be offset by using bidentate pyridyl ligands, tethered by a linker at the 3-position as has been demonstrated for Pt(II) bis alkyl complexes [14].

Conclusions

We have demonstrated separate tuning of the LUMO and HOMO orbital energies within the [Pt(4-CO_2CH_3-py)$_2$(mnt)] **3b**, [Pt(4-NO_2-py)$_2$(mnt)] **3c** and [Pt(4-CO_2CH_3-py)$_2$(dmit)] **4b** complex series by separately altering the substituted-pyridyl and the dithiolate ligand. This allowed us to shift the lowest energy transition into the visible spectrum, essential for any subsequent use of such complexes in solar energy conversion. The UV/Vis and EPR spectra of the reduced compounds are consistent with the reduction electrons entering two separate pyridyl based orbitals. Thus, replacing the 4-CO_2CH_3-py ligands in [Pt(4-CO_2CH_3-py)$_2$(mnt)] with two 4-NO_2-py ligands, shifts the pyridyl reductions to more positive potentials and decreases the oxidation-reduction energy gap. Although there is some increase in visible absorption of **4b** compared with **3b** however, the HOMO – LUMO+2 character of the lowest-energy intense absorption limits the extent of any redshift due to the negligible nitro contribution to the LUMO+2 orbital. We have explored the potential of such complexes for solar energy conversion in devices such as the dye-sensitised solar cell. Poor binding to TiO_2 through nitro groups and possible low stability of the complexes may limit their current utility, suggesting use of nitro groups as anchors may be better suited when combined with other anchoring groups.

Experimental

Methyl isonicotinate (4-CO_2CH_3-py), isonicotinic acid (4-CO_2H-py) and 4-nitropyridine N-oxide purchased from Sigma-Aldrich/Fluka and K_2PtCl_4 provided by Johnson Matthey were used as received. Na_2(mnt) [15] and (C_6H_5OC)$_2${1,3-dithiol-2-thione-4,5-dithiolate} (PhCO)$_2$dmit [16] were prepared as previously reported.

Synthesis of [Pt(4-CO_2H-py)$_2$(dmit)] 4a. Na metal (10.7 mg, 0.46 mmol) was added to 100ml of dry MeOH under N_2 to make 2 molar equivalents of NaOMe. (PhCO)$_2$-dmit (94 mg, 0.23 mmol) was ground up and added to this solution until all the solid had dissolved and the solution was deep red in colour [17]. [$PtCl_2$(4-CO_2H-py)$_2$] (119 mg, 0.20 mmol) was dissolved in dry DCM (50 mL) and to this was added the Na_2dmit solution dropwise over 10 minutes. This was stirred at room temperature for 2 hours under N_2. The solvent was reduced to 20 % *in vacuo* (with no heating). Isopropyl alcohol (~50 ml) was added and the solution was

left in the freezer until a precipitate formed, which was removed by centrifugation. The remaining supernatant solution was decanted and reduced *in vacuo* to give the desired product. Yield: 35 % (47 mg, 0.07 mmol); Anal. Calc. for $PtS_5N_2O_4C_{15}H_{10}$; C, 28.26; H, 1.57; N, 4.40. Found: C, 28.35; H, 1.60; N, 4.39; ^{1}H NMR (250 MHz, DMSO-D6): δ7.7 (4H, d), δ8.6 (4H, d).

Synthesis of [Pt(4-CO_2CH_3-py)$_2$(dmit)] 4b. Na metal (8 mg, 0.35 mmol) was added to 100ml of dry MeOH under N_2 to make 2 molar equivalents of NaOMe. $(PhCO)_2$dmit (68 mg, 0.17 mmol) was ground up and added to this solution until all the solid had dissolved and the solution was deep red in colour [17]. [$PtCl_2$(4-CO_2CH_3-py)$_2$] [11] (91.0 mg, 0.17 mmol) was dissolved in dry DCM (50 mL) and the Na_2dmit solution added to this dropwise over 10 minutes. This was stirred at room temperature for 2 hours under N_2. The solvent was reduced to 20 % *in vacuo* (with no heating) and the remaining solution was left overnight in the fridge. The resulting precipitate was collected using filtration. Anal. Calc. for $PtS_5N_2O_4C_{17}H_{14}$; C, 30.68; H, 2.11; N, 4.21. Found: C, 29.30; H, 2.03; N, 4.84; ^{1}H NMR (250 MHz, $CDCl_3$): δ8.9 (4H, d), δ8.4 (4H, d), δ4.0 (6H, s).

Synthesis of 4-NO_2-py 1c. This was prepared using a known synthesis [18]. Yield: 81 % (0.3 g, 2.4 mmol); Anal. Calc. for $C_5H_4N_2O_2$; C, 48.39; H, 3.25; N, 22.58. Found: C, 48.25; H, 3.12; N, 22.35; ^{1}H NMR (250 MHz, DMSO-d6): δ8.0 (2H, dd), δ8.9 (2H, dd).

Synthesis of [$PtCl_2$(4-NO_2-py)$_2$] 2c. $K_2[PtCl_4]$ (130 mg, 0.313 mmol) and 4-NO_2-py (216 mg, 1.74 mmol) were refluxed in deionised water (50 mL) for an hour. The yellow precipitate was then filtered and washed with diethyl ether and dried in a vacuum. This was then recrystallised from a hot saturated solution of DMF. Yield: 52 % (83 mg, 0.163 mmol); MS (FABMS) *m/z*: 515 $\{M\}^+$; Anal. Calc. for $PtCl_2N_4O_4C_{10}H_8.2H_2O$; C, 21.81; H, 2.18; N, 10.18; Found: C, 21.72; H, 1.11; N, 9.53. ^{1}H NMR (250 MHz, $CDCl_3$): δ9.0 (4H, d), δ8.0 (4H, t).

Synthesis of [Pt(4-NO_2-py)$_2$(mnt)] 3c. A solution of [$PtCl_2$(4-NO_2-py)$_2$] (200 mg, 0.389 mmol) was dissolved in dry DCM (50 mL) and Na_2(mnt) (72.3 mg, 0.389 mmol) dissolved in dry MeOH (20 mL) were mixed together and stirred under N_2 for 2 hours. The solvent volume was reduced to 20 % *in vacuo* (avoiding any heating) and the remaining solution was left overnight in the fridge. The precipitate was collected by filtration. Yield: 68 % (154 mg, 0.264 mmol); Anal. Calc. for $PtS_2N_6O_4C_{14}H_8.4CH_3OH$; C, 30.38, H, 3.38; N, 11.81. Found: C, 32.21; H, 1.39; N, 9.93. ^{1}H NMR (250 MHz, DMSO-d6): δ8.1 (dd), δ8.9 (m).

Other Experimental Information. All UV/vis spectra were recorded on a Perkin-Elmer Lambda 9 spectrophotometer controlled by a Datalink PC, running UV/Winlab software. Electrochemical studies were carried out using a DELL GX110 PC with General Purpose Electrochemical System (GPES), version 4.8, software connected to an autolab system containing a PGSTAT 30 or Type III potentiostat.

The techniques used a three-electrode configuration, with a 0.5mm diameter Pt disc working electrode, a Pt rod counter electrode and an Ag/AgCl (saturated KCl) reference electrode against which the ferrocenium/ferrocene couple was measured to be +0.55V. The supporting electrolyte was 0.1 M tetrabutylammonium tetrafluoroborate ($TBABF_4$). OTTLE (Optically Transparent Thin Layer Electrode) measurements were taken using a quartz cell of pathlength 0.5 mm, a Pt/Rh gauze working electrode, an Ag/AgCl reference electrode and a Pt wire counter electrode [19]. UV/vis spectra were recorded on a Perkin-Elmer Lambda 9 spectrophotometer, controlled by a Datalink PC, running UV/Winlab software. Measurements on samples were carried out at 233 K in DMF/$TBABF_4$ (0.1 M) was used as the supporting electrolyte in all cases. Electron Paramagnetic Resonance spectra were taken using a flat cell, a Pt/Rh gauze working electrode, an Ag/AgCl reference electrode and a Pt wire counter electrode and radical species were generated using a BAS CV-27 voltammograph. EPR spectra were recorded on an X-band Bruker ER200D-SCR spectrometer connected to a Datalink 486DX PC with EPR Acquistion System, version 2.42 software. The temperature was controlled by a Bruker ER4111 VT variable temperature unit. All g values were corrected to 2,2'-diphenyl-1-picrylhydrazyl with $g_{literatue} = 2.0036 \pm 0.0002$ [20]. Measurements on samples were carried out at 233 K in DMF. $TBABF_4$ (0.1 M) was used as the supporting electrolyte except where indicated. DFT calculations were run using Gaussian 03, Revision D.01 [21], The images were generated using Arguslab [22]. 6-31G* basis set was used for the C, N, H, O, Cl and S atoms and the Hay-Wadt VDZ (n+1) ECP basis sets for the Pt(II) centre [23].

References

[1] S. D. Cummings, R. Eisenberg, *J. Am. Chem. Soc.*, 118 (1996) 1949.

[2] M. Hissler, J. E. McGarrah, W. B. Connick, D. K. Geiger, S. D. Cummings, R. Eisenberg, *Coord. Chem. Rev.*, 208 (2000) 115.

[3] J. Zhang, P. Du, J. Schneider, P. Jarosz, R. Eisenberg, *J. Am. Chem. Soc.,* 129 (2007) 7726.

[4] C.Makedonas, C. A. Mitsopoulou, *Eur. J. Inorg. Chem.,* (2006) 590.

[5] A. Islam, H. Sugihara, K. Hara, L. P. Singh, R. Katoh, M. Yanagida, Y. Takahaski, S. Murata, H. Arakawa, *New J. Chem.*, 24 (2000) 343.

[6] A. Islam, H. Sugihara, K Hara, L. P. Singh, R. Katoh, M. Yanagida, Y. Takahaski, S. Murata, H. Arakawa, *Inorg. Chem.*, 40 (2001) 5371.

[7] E. A. M. Geary, L. J. Yellowlees, L. A. Jack, I. D. H. Oswald, S. Parsons, N. Hirata, J. R. Durrant, N. Robertson, *Inorg. Chem.*, 44 (2005) 242.

[8] A. M. Geary, K. L. McCall, A. Turner, P. R. Murray, E. J. L. McInnes, L. J. Yellowlees, N. Robertson, *Dalton Trans,* (2008) 3701.

[9] B. O'Regan, M. Grätzel, *Nature*, 353 (1991) 737; Md. K. Nazeeruddin, M. Grätzel, *Comp. Coord. Chem. II,* 9, (2003) 719-758.

[10] N. Roberston, *Angew. Chem. Int. Ed.,*45 (2006) 2338-2345.

[11] L. P. Moorcraft, A. Morandeira, J. R. Durrant, J. R. Jennings, L. M. Peter, S. Parsons, A. Turner, L. J. Yellowlees, N. Robertson, (2008) 6940.

[12] C. Makedonas, C. A. Mitsopoulou, *Eur. J. Inorg. Chem.*, (2006) 2460; C. Makedonas, C. A. Mitsopoulou, F. J. Lahoz, A. I. Balana, *Inorg. Chem.,* 42 (2003), 8853; C. Makedonas, C. A. Mitsopoulou, *Inorg. Chim. Acta.,* 360 (2007) 3997.

[13] M. Itoh, T. Okamoto, S. Nagakura, *Bull. Chem. Soc. Jpn.,* 36 (1962) 1665.

[14] F. Zhang, C. W. Kirby, D. W. Hairsine, M. C. Jennings, R. J. Puddephatt, *J. Am. Chem. Soc.,* 127 (2005) 14196.

[15] G. Markl, R. Vybiral, *Tetrahedron Lett.* 30 (1989) 2903.

[16] G. Steimecke, H. J. Sieler, R. Kirmse, E. Hoyer, *Phosphorus and Sulfur*, 7, (1979), 49.

[17] C. E. Keefer, S. T. Purrington, R. D. Bereman, B. W. Knight, J. Bedgood, R. Danny, P. D. Boyle, *Inorg. Chim. Acta,*282 (1998) 200.

[18] R. Ochiai, *J. Org. Chem.*, 18 (1953) 534.

[19] S. A. McGregor, E. J. L. McInnes, R. J. Sorbie, L. J. Yellowlees, *Molecular Electrochemistry of Inorganic, Bioinorganic and Organometallic Compounds*; Kluwer: Dordrecht, The Netherlands, 1992.

[20] S. A. Al'tshuler, B. M. Kozyrev, *Electronic Paramagnetic Resonance*, Academic Press: New York, **1964**.**1993**; p 503, 1964.

[21] M. J. Frisch, G. W. Trucks, H. B. Schlegel, G. E. Scuseria, M. A. Robb, J. R. Cheeseman, J. A. Montgomery, J. T. Vreven, K. N. Kudin, J. C. Burant, J. M. Millam, S. S. Iyengar, J. Tomasi, V. Barone, B. Mennucci, M. Cossi, G. Scalmani, N. Rega, G. A. Petersson, H. Nakatsuji, M. Hada, M. Ehara, K. Toyota, R. Fukuda, J. Hasegawa, M. Ishida, T. Nakajima, Y. Honda, O. Kitao, H. Nakai, M. Klene, X. Li, J. E. Knox, H. P. Hratchian, J. B. Cross, V. Bakken, C. Adamo, J. Jaramillo, R. Gomperts, R. E. Stratmann, O. Yazyev, A. J. Austin, R. Cammi, C. Pomelli, J. W. Ochterski, P. Y. Ayala, K. Morokuma, G. A. Voth, P. Salvador, J. J. Dannenberg, V. G. Zakrzewski, S. Dapprich, A. D. Daniels, M. C. Strain, O. Farkas, D. K. Malick, A. D. Rabuck, K. Raghavachari, J. B. Foresman, J. V. Ortiz, Q. Cui, A. G. Baboul, S. Clifford, J. Cioslowski, B. B. Stefanov, G. Liu, A. Liashenko, P. Piskorz, I. Komaromi, R. L. Martin, D. J. Fox, T. Keith, M. A. Al-Laham, C. Y. Peng A. Nanayakkara, M. Challacombe, P. M. W. Gill, B. Johnson, W. Chen, M. W. Wong, C. Gonzalez, J. A. Pople, Inc., G. *Gaussian 03*, Revision D.01; Wallingford CT, 2004.

[22] ArgusLab 4.0.1 Mark A. Thompson Planaria Software LLC, Seattle, WA http://www.arguslab.com

[23] P. J. Hay, W. R. Wadt, *J. Phys. Chem.*, 82 (1985) 299.